In-flight absolute radiometric calibration for thermal infrared band of HJ-1B

HAN Qijin[1,2], **MIN Xiangjun**[2], **FU Qiaoyan**[2]

1. *China Academy of Space Technology*, *Beijing* 100081, *China*;
2. *China Center for Resources Satellite Date and Application*, *Beijing* 100094, *China*

Abstract: This paper presentes an in-flight site calibration method for thermal infrared band of HJ-1B, taking advantages of Lake Qinghai test-site for the absolute radiometric calibration for thermal infrared band of HJ-1B. By using measurement data and landsat5-TM to analyze the different results between site calibration and primeval calibration, it shows that the accuracy of in-flight site calibration had been increased 0.6%—3% comparing with the primeval calibration result and the total accuracy is about 1K. Thus this new site calibration method is applicable to the in-flight absolute radiometric calibration of these sensors without the capability of detecting cold space. By the way, the accuracy of calibration for thermal infrared of HJ-1B can meet user's requirements for the application of quantitative thermal infrared data.

Key words: HJ-1B, thermal infrared, site calibration, accuracy

CLC number: TP722.5 **Document code:** A

Citation format: Han Q J, Min X J and Fu Q Y. 2010. In-flight absolute radiometric calibration for thermal infrared band of HJ-1B. *Journal of Remote Sensing*. **14**(6): 1212—1225

1 INTRODUCTION

With the development of remote sensing technology in recent years, thermal infrared remote sensing also finds its broader quantitative application. Thermal infrared remote sensing plays an important role in the prevention of environmental pollution, natural disaster surveillance, agricultural draught surveillance, UHI research and so on(Tian *et al.,* 2006). China successfully launched environment disaster surveillance and forecast satellites (for short HJ-1 satellite) on Sep. 6th, 2008, which carries a thermal infrared MSS (for short IRS). This sensor features 10.5μm—12.5μm channel width, 300 Nadir spatial resolution, 720km breadth and it repeats observation every four days. All of this, to some extent, can meet the requirements of thermal infrared quantitative application.

The precondition of remote sensing data quantitative application is the exact absolute radiometric calibration for sensor, that is, the quantitative relationship between output signals of sensor (usually satellite image digital counts DN) and target output of absolute physics quantity(Palmer,1993). All of the diversification factors cause degradation in detestability of satellite sensors; including sensor's vibration when launched, space condition change in orbit, degradation of parts of an apparatus and so on. Regular in-flight absolute radiometric calibration can check up sensor's changing performance, modify primeval calibration resu- lts, and finally meet the accurate requirements of remote sensing quantitative application (Biggar, 1990).

In-flight absolute radiometric calibration methods include on-boar d-calibration, cross-calibration and site-calibration. The site-calibration can test the stability of onboard-calibration system, correct accur acy of onboard calibration results, and achieve the purpose of calibration without reference data of cross-calibration. At present, site-calibration methods of thermal infrared is proposed for Landsat5-TM, MODIS, FY satellite sensors, using homogeneous objects such as ocean, lakes, cloud (Richter, 1997; Teillet & Slater *et al.,* 1990). Those methods have different characteristics and applicability.

This paper has done research on the characteristics of IRS the capability of detecting cold space, and then without carried out in-flight site radiometric calibration for B8 channel of HJ-1B.The paper obtained an improved site-calibration and calibration result based on Lake Qinghai measurements on Aug.12th, 2009. Furthermore, the accuracy of this calibration result is analyzed using test site-measuring temperatures and Landsat5-TM. The final result indicates that site-calibration result is accurate and it can supply user for engaging on remote sensing data quantitatively application with calibration coefficients (www. cresda.com).

2 IN-FIGHT SITE-CALIBRATION METHOD

By detecting calibration site (Lake Qinghai), the satellite

Received: 2009-12-07; **Accepted**: 2010-04-08
Foundation: National major technology project for special engineering (No.KGJ [2006]785).
First author biography: HAN Qijin (1983—) male. He got his master degree in China Academy of Space Technology, Beijing, China. He is focusing on the research of sensor radiometric calibration and quantitatively application. E-mail: cresda_hanjin@sina.com

sensors receives three radiance including three parts: the radiance directly from earth's surface that reaches the sensor through atmospheric scattering and absorption; the size of which is decided by the temperature of water surface, land surface emissivity and atmospheric transmission; The up-welling atmospheric radiance that is related to the contents and physical state of Air Impact factor; the down-welling radiance reflected by water surface that reaches the sensor through atmospheric scattering and absorption(Zhang, 2006).

The Monochromatic radiance which is received at HJ-1B sensor radiance can be calculated by the following equation:

$$L(\lambda) = L_{\text{lake}}(\lambda)\tau_a(\lambda) + L_{\text{up}}(\lambda) + \rho_{\text{lake}}(\lambda)\tau_a(\lambda)L_{\text{down}}(\lambda) \quad (1)$$

where $\tau_a(\lambda)$is the total transmission rate of the atmosphere, $L_{\text{lake}}(\lambda)$ is the water body radiance to the direction of the satellite; $L_{\text{up}}(\lambda)$ is the up-welling Monochromatic radiance; $\rho_{\text{lake}}(\lambda)$ is the water body reflectance; $L_{\text{down}}(\lambda)$ is the down-welling radiance.

Being a blackbody system, the lake surface radiance emitted and reflected could be united into $L_{\text{lake2}}(\lambda)$ and could be measured by spectrum radiometer CE312. Then Eq. (1) changes Eq. (2).

$$L(\lambda) = L_{\text{lake2}}(\lambda)\tau_a(\lambda) + L_{\text{up}}(\lambda) \quad (2)$$

The total Monochromatic at-sensor radiance must be transformed into satellite channel equivalent radiance, the equivalent radiance of HJ-1B channel can be defined as $L_e(\lambda)$.

$$L_e = \frac{\int L(\lambda) f_{\text{IRS}}(\lambda) d\lambda}{\int f_{\text{IRS}}(\lambda) d\lambda} \quad (3)$$

where $f_{\text{IRS}}(\lambda)$ is spectral response function of HJ-1B-B8 channel. The relationship between HJ-1B-B8 channel radiance and sensor digital counts is designed in linearity, so it can be supposed the following equation:

$$\text{DN} = g \times L_e + b \quad (4)$$

where *DN* is the sensor digital counts; L_e is channel radiance; the calibration coefficient g is gain and b is the offset. When sensors observe land surface and cold space comparatively, we can conclude two groups of different data. At the same time, the calibration result is calculated based on Eq. (4). Because radiometric calibration of HJ-1B-IRS is not capable of observing cold space, we uses onboard high-temperature cali- bration blackbody data in replace. The site-calibration of HJ-1B thermal infrared flow chart is shown in Fig.1.

3 SITE-CALIBRATION FOR THERMAL INFRARED OF HJ-1B

3.1 Lake Qinghai Site Descriptions and data measurements

Lake Qinghai (Qinghai province), the biggest inland Plateau salty lake in China, is located in the northeast part of Qingzang Plateau. The coordinates of the test are 36.5°N—37.2°N latitude and 99.6°E—100.7°E longitude. The size of Lake Qinghai is approximately 4473km^2 with a circumference of 360km. A length of 109km in east and west, a width of 65km in south and north and an average depth of 16km. The deepest place of Lake Qinghai is 28km with the sea level of 3196km. This site is a natural site-calibration for thermal infrared of HJ-1B, which belongs to high frigid semiarid grassland weather and is characterized by high sea level, clean air, small aerosol particles, low water vapor and balanced water temperature (Li *et al.,* 2001).

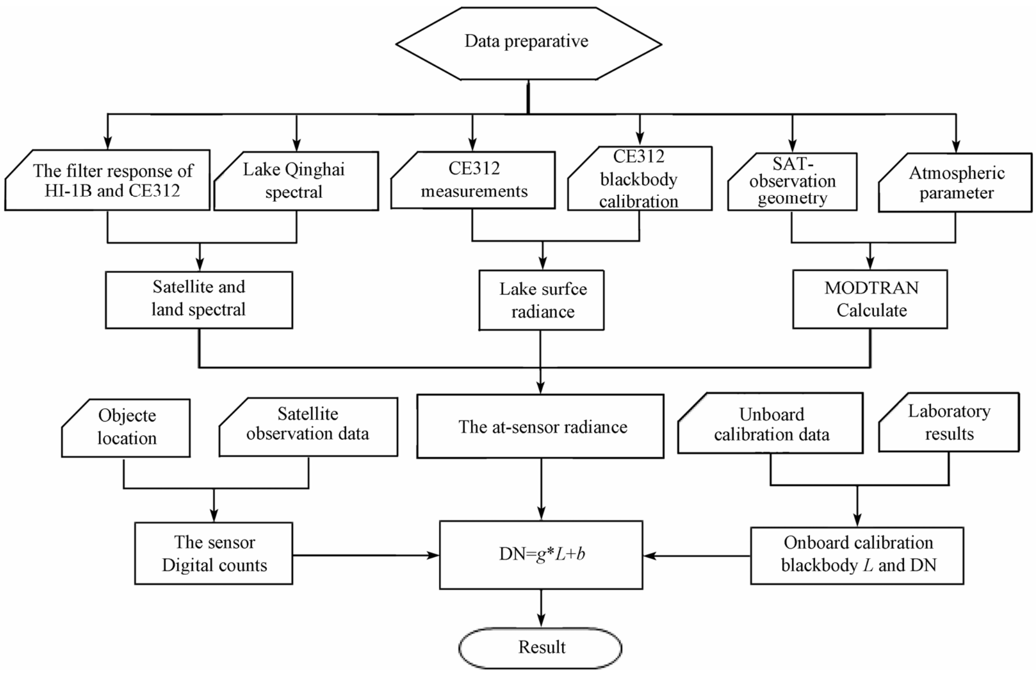

Fig. 1 In-flight site calibration for thermal infrared channel of HJ-1B

The test of site-calibration for thermal infrared of HJ-1B measurements includes Lake Qinghai surface radiance (CE312 measured), Lake spectral data (102F measured), lake water temperature, GPS, universal atmospheric parameter and so on.

3.2 CE312 lake radiance processing

3.2.1 Radiometer blackbody calibration

The blackbody calibration of the principle of radiometer CE312 is realized by a secluded reflector comparing the object radiance and interior reference radiance. This test uses Boman M340 Blackbody to calibrate CE312, and obtains many group calibration data at 5F1t1M model, and then calculates the calibration coefficients A and B based on relationship between radiometer digital counts and object radiance Eq.5.

$$L_s - L_m = A \times (DC_m - DC_s) + B \tag{5}$$

where DC_m is the digital count of radiometer when reflector is inserted into light-wave path and when the reflector is taken over, L_s is Boman M340 blackbody radiance, L_m is the reflector radiance.

Blackbody radiance L_s and reflector radiance L_m are calculated with blackbody temperature T_s, radiometer interior probe temperature T_m, Plank Eq.6 and Eq.7.

$$L_\lambda = \frac{C_1}{\lambda^5 \left(e^{C_2/\lambda T} - 1 \right)} \tag{6}$$

$$L = \frac{\sum_{i=0}^{N} [L_\lambda \times (\lambda_{i+1} - \lambda_i) \times f(\lambda_i)]}{\sum_{i=0}^{N} [(\lambda_{i+1} - \lambda_i) \times f(\lambda_i)]} \tag{7}$$

where L_λ is the blackbody radiance, $C_1=1.19104\times10^8$ w·μm^4·m^{-2}·sr^{-1}, $C_2=1.43877\times10^4$ μm·K, T is the blackbody temperature.

According to the feature of thermal infrared channel of HJ-1B, the calibration for fifths channel of CE312 is needed. The calibration blackbody was plane blackbody with emissivity 0.98±0.01, temperature error ±0.2°C, and reading error ±0.2°C,so that there will be certain error with single calibration data. Data processing required averaging the same temperature data and calculated calibration coefficients. The blackbody calibration results of CE312 in Lake Qinghai test are as follows, A:0.0025, B:0.0184 W·m^{-2}·sr^{-1}·μm^{-1}.

3.2.2 Lake Qinghai radiance calculation

Due to the above blackbody calibration results, the radiance of test-site measured by CE312 is performed. The lake radiance L_s and temperature T are obtained with Eq.5 and Eq.6. Owing to the errors under the measurement, we need to eliminate those singularity data. The processed introductions in detail are as follows:

(1) Calculate every-station brightness temperature (T_i, i=1, 2, ..., n) with Plank equation.

(2) Calculate average brightness temperature T_a.

$$T_a = (\sum_{i=1}^{n} T_i)/n \tag{8}$$

(3) Deviation average between T_i and T_a.

$$\delta T_a = (\sum_{i=1}^{n} |T_i - T_a|)/(n-1) \tag{9}$$

(4) Eliminate accidental singularity with the following relation.

$$\frac{|T_i - T_a|}{\delta T_a} \geqslant 3 \tag{10}$$

Lake temperature with CE312 measurements retrieval was compared with continuous-temperature measuring apparatus data to validate rationality and accuracy of data processing. Comparison result is shown in Fig.2.

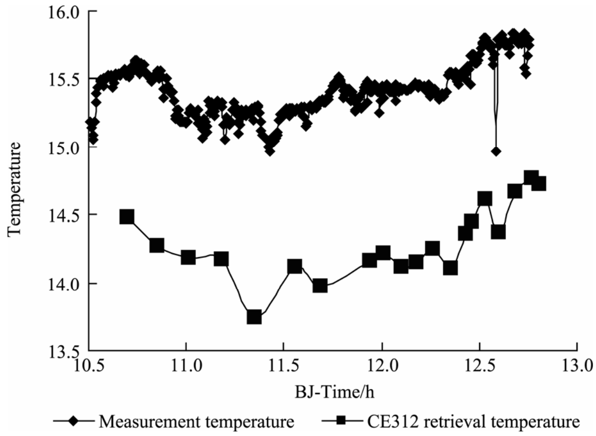

Fig. 2 Comparation between CE312 retrieval temperature and measurement temperature

The trends of temperature-line between CE312 retrieval temperature and continuous-measuring temperature are the same and the average temperature variation is less than 1.2°C.

The continuous thermo scope is 0.02°C in precision, and located in 0.5m under the water body. The lake Qinghai is saline and the temperature is converse delaminated in autumn. Considering salinity and illumination, we find the measured temperature is less than 0.2°C (Fang Shenghui *et al.,* 2009). The data of radiometer CE312 was bigger than actual temperature for water reflection and emissivity is 0.98. Considering the homogeneous of Lake Qinghai and 0.6 W·m^{-2}·sr^{-1}·μm^{-1} in precision, the CE312 result satisfies the requirements of sensor calibration (Zhu Li, 2008). After eliminating error data, average lake radiance is half an hour during the satellite passing through: 7.7289 W·m^{-2}·sr^{-1}·μm^{-1}.

3.3 Spectral matching

There are spectral differences between CE312 channel and thermal infrared channel of HJ-1B, because radiometer is designed simulating by satellite channels. Spectral matching between CE312-B5 and HJ-1B-B8 can minify the differentia.

Particular steps are shown as follows. Convolution of 102F-surface radiance with the CE312 response the function to obtain lake-surface radiance; Convolution of 102F-surface radiance with the IRS response the function to obtain IRS-lake-surface radiance. Calculate the ratio between the CE312-surface radiance and IRS-surface radiance.

$$R_{CE} = \frac{\int L_{102f}(\lambda) \cdot f_{CE}(\lambda) d\lambda}{\int f_{CE}(\lambda) d\lambda} \tag{11}$$

$$R_{IRS} = \frac{\int L_{102f}(\lambda) \cdot f_{IRS}(\lambda) d\lambda}{\int f_{IRS}(\lambda) d\lambda} \tag{12}$$

$$k = \frac{R_{IRS}}{R_{CE}} \tag{13}$$

where L_{CE} is CE312 measured lake-surface radiance, L_{IRS} is IRS lake-surface radiance, $L_{102f}(\lambda)$ is 102F measured lake- surface radiance, $f_{CE}(\lambda)$ is CE312-band5 response function, $f_{IRS}(\lambda)$ is IRS system response function.

The comparison of the response function between CE312-band5 and HJ-1B satellite thermal infrared channel is shown in Fig.3.

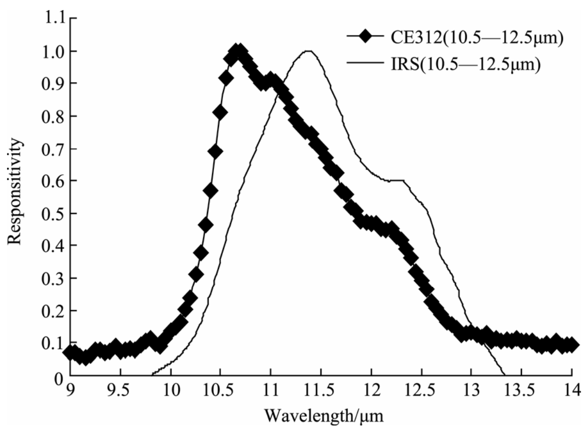

Fig. 3 The response function of CE312-band5 and IRS thermal infrared channel

This paper selects 102F data as reference and calculates the arithmetical average of different matching results in processing. Thus the spectral matching result of HJ-1B satellite B8 channel is 1.01, and the at-sensor radiance can be calculated by the following equation:

$$L_e(\lambda) = k \cdot L_{lake2}(\lambda) \cdot \tau_a(\lambda) + L_{up}(\lambda) \tag{14}$$

3.4 MODTRAN radioactive transfer calculate

Atmospheric characteristic data are collected at the same time as the in-situ measurements. The temperature, water vapor and pressure altitude profile and the earth's surface parameters can be extracted from the measurements. Considering testing condition, the position of sounding balloon blastoff was near the bird- island hotel.

The curve of atmospheric temperature, water vapor and pressure along with altitude is shown in Fig.4.

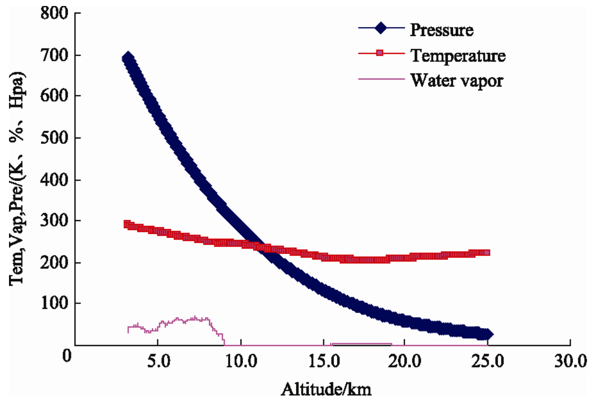

Fig. 4 Atmospheric characteristic curve

These atmospheric and observation geometry data were input to MODTRAN radioactive transfer model (Berk A & Anderson G.P *et al.,* 1999) that computes total surface-to- satellite path transmittance and path thermal radiance which are shown in Fig.5.

The equivalent satellite channel of total transmittance and equivalent path thermal radiance were calculated by integrating over the system response function of IRS thermal infrared channel. The equivalent transmittance are 0.8813 without units, and the equivalent path thermal radiance is 0.7225 $W \cdot m^{-2} \cdot sr^{-1} \cdot \mu m^{-1}$.

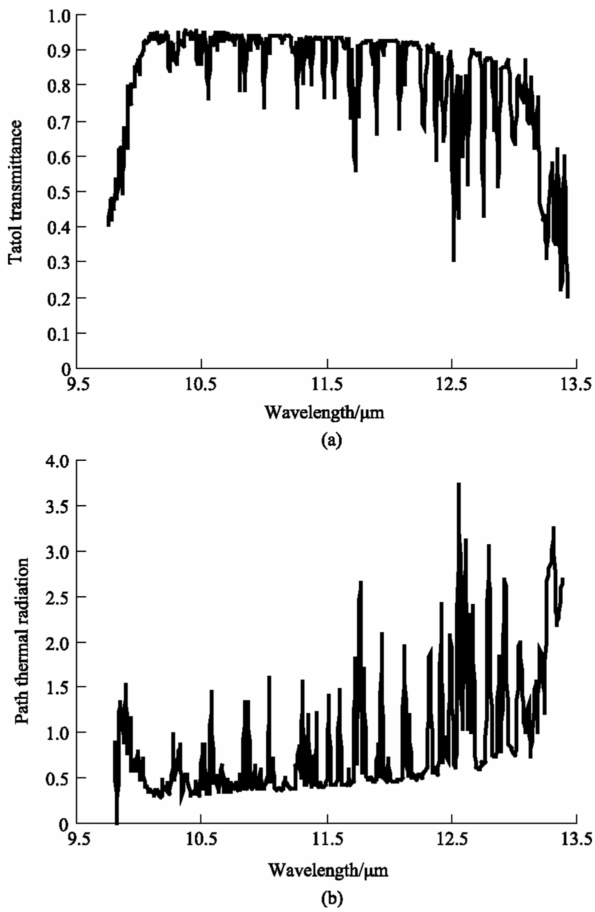

Fig. 5 Atmospheric radiance transmission
(a) Atmospheric total transmittance; (b) Atmospheric path thermal radiance

3.5 Determination of image digital numbers (DN) and calibration coefficients

To extract the digital numbers of images, we must ensure the matching precision between measurements region and extraction region. The DN output was determined by averaging the DN output for the requirement pixels related to our test site(Mayumi Y & Hiroshi M.K *et al.,* 2005). The region near our measure site was located in north of the Hill-Haixin by GPS data which were measured in test. The extraction region is shown in Fig.6.

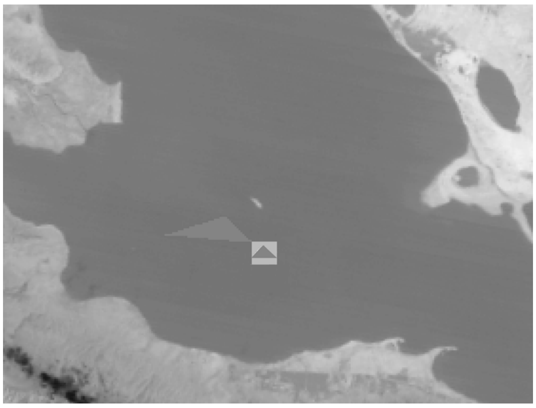

Fig. 6 Extraction of image digital numbers

The DN from these pixels is the averaged and rated to the predicted radiance from the primeval Eq. (1) calculated with measurements to obtain the calibration coefficients using Eq. (3). There are two unknown quantities in Eq. (3), so it is necessary to obtain another group of data. The IRS doesn't have capability to observe the cold space on-orbit. Meanwhile, the IRS is designed in linearity, so error of the single arithmetic is biggish. On-board high-temperature blackbody was adopted to replace cold space data.

At the basis of the on-board calibration principle, the high-temperature blackbody data processing results are shown in Table.1.

Table 1 The result of onboard high-temperature blackbody data processing

Time/Item	Aug.5th		Aug.14th	
	DN	Radiance/ ($W\cdot m^{-2}\cdot sr^{-1}\cdot \mu m^{-1}$)	DN	Radiance/ ($W\cdot m^{-2}\cdot sr^{-1}\cdot \mu m^{-1}$)
Min	677.25	11.99	680.62	12.00
Max	718.87	12.99	720.00	13.02
Average	699.82	12.21	701.52	12.23

According to the results presented above, calibration coefficients for thermal infrared channel of HJ-1B are calculated. The gain is 59.421 $W\cdot m^{-2}\cdot sr^{-1}\cdot \mu m^{-1}$. The offset is –25.441.

4 RESULT ANALYSIS AND DISCUSSION

4.1 Calibration result precision verify

The paper selected Lake Qinghai temperature measurements and Landsat5-TM (10.5—12.5μm) to cross verify the primeval result and the new site-calibration result.

4.1.1 Analyzing based on actual measurements

In order to obtain the simultaneously and coprovincial water surface radiance, we calibrated the remote sensing images in Aug.12th, Aug.16th with the primeval coefficients and the new coefficients. And then, compared the temperature measurements with the brightness temperatures of HJ-1B data, which were calculated by radioactive transfer model arithmetic, we can obtain the result. (Table 2).

Table 2 Comparison result temperature retrieval for HJ-1B and the measurements

Time	Coefficients	Retrieval Temperature/°C	Continuous temperature differentia /°C	Buoyage temperature differentia /°C
Aug.12th	primeval	15.99	0.65	1.14
	New	15.43	0.10	0.58
Aug.16th	primeval	15.86	0.31	0.39
	New	15.28	0.27	0.19

4.1.2 Analyzing based on Landsat5-TM

For the list range limitation, the data were selected from Lake Qinghai TM on Aug.11th 2009, the satellite HJ-1B and the satellite Landsat5-TM and compared as the reference data to analyze the calibration result. Because the same color means the matching regions between the two satellites' images (Fig.7), the DN statistics of the regions can be achieved (Table 3).

Table 3 Matching regions DN statistics of HJ-1B and Landsat5-TM

Region	HJ-1B thermal infrared data DN statistics			Landsat5-TM DN statistics		
	Min	Max	Mean	Min	Max	Mean
1	428	443	435.05	115	117	115.83
2	426	444	434.74	115	117	116.06
3	426	441	433.93	115	117	115.93
4	421	441	432.60	112	117	115.08
5	423	439	431.81	114	116	115.18

We calculate the absolute radiometric calibration equation by assistant file of Landsat5-TM.

$$L_e = \frac{(L_{max} - L_{min})}{255} \times DN + L_{min} \qquad (15)$$

where L_{max}=15.303, L_{min}=1.238.

At the basis of the DN statistics, we calculate the radiance and the brightness temperatures, and then, make the average of the results to increase precisions. The brightness temperatures of HJ-1B data are compared with BTS of Landsat5-TM.

Compared with Landsat5, HJ-1B passed through Lake Qinghai is12 minutes early. However, we assume the temperature invariableness, considering water area and quality. The spectral range of these two sensors is similar, so the comparison

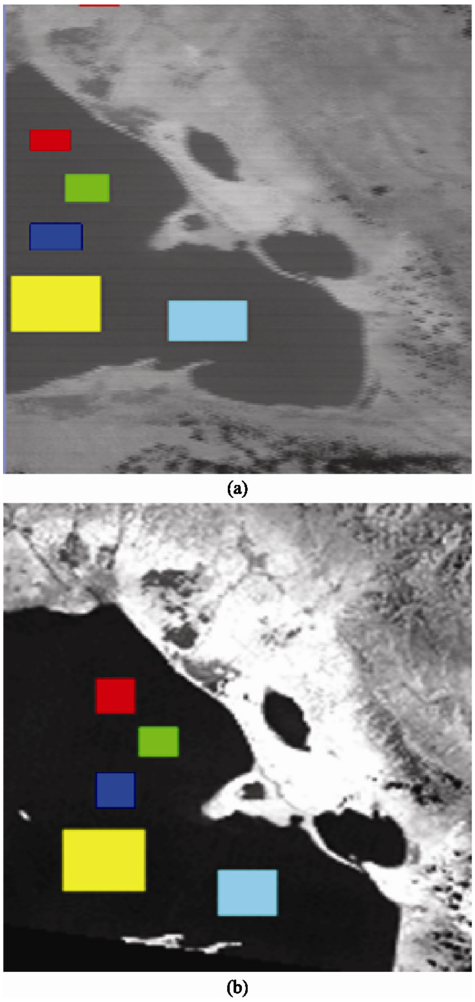

Fig. 7 The spatial matching region of HJ-1B and Landsat5-TM
(a) The spatial matching region of HJ-1B; (b) The spatial matching region of Landsat 5-TM

results can reflect the accuracy of different coefficients(Flavio & Jurandir 2004). After analyzing Table.4, we conclude the radiance and BTS based on site-calibration result close to Landsat5-TM product (Kurtis & Dennis *et al.,* 2004).

Table 4 Radiance and brightness temperature comparison

Data with calibrated coefficients	Primeval	Site-calibration	Landsat5-TM
Radiance / $W \cdot m^{-2} \cdot sr^{-1} \cdot \mu m^{-1}$	7.7795	7.7257	7.6150
Brightness temperature / °C	15.18	14.73	14.15
Radiance Stdev	0.00052	0.00055	0.00062

4.2 Different calibration results accuracy analysis

4.2.1 Primeval calibration coefficients accuracy analysis

The primeval calibration for thermal infrared of HJ-1B was obtained by on-board blackbody calibration in 2008. What is more, the arithmetic for the pre-launch laboratory's experience has errors. At the same time, there are some influence factors such as space environment, components disintegration and so on. The primeval calibration result has not reflected the right relationship between input information and digital number of HJ-1B-IRS. It is very important to correct calibration accuracy.

4.2.2 Site-calibration result accuracy analysis

The site-calibration for thermal infrared channel of HJ-1B is influenced by many factors. Firstly, the Lake Qinghai surface radiance fluctuates with time and temperature changing (Fig.8). Synthetically analyzing, there is about 0.5 $W \cdot m^{-2} \cdot sr^{-1} \cdot \mu m^{-1}$ changes in an hour. The different spectral response of CE312-B5 and HJ-1B-B8 channel along with matching standard data fluctuation bring spectral matching errors (Simon J.H & Gyanesh *et al.,* 2004).

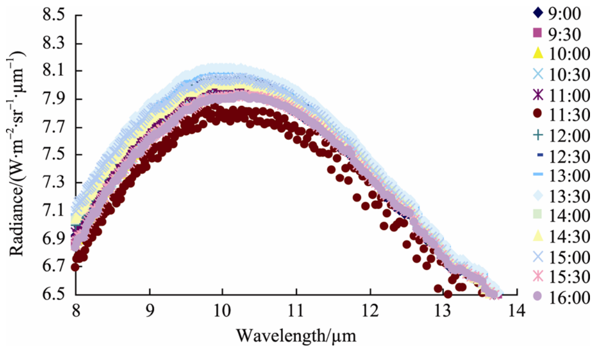

Fig. 8 Radiance fluctuation curve of Lake Qinghai

Secondly, detecting stability of sensor make on-board calibration blackbody temperature change ±2°C, which causes radiance 0.02($W \cdot m^{-2} \cdot sr^{-1} \cdot \mu m^{-1}$) and digital number 2DN in fluctuate. In summarize, on-board high-temperature calibration blackbody data causes site-calibration of HJ-1B B8 channel a few errors.

4.2.3 Comparison of calibration result accuracy

According to the comparative results above, we analyze the accuracy change between primeval result and site-calibration result of HJ-1B thermal infrared channel.

The new calibration coefficients are better than 0.6%—3% in relative precision, comparing with the primeval result. Furthermore, the analyzing result shows that the detection capability have changed, and needed to be corrected periodically.

5 CONCLUSION

This paper offers a new in-flight site absolute radiometric calibration method for thermal infrared channel of HJ-1B on the basis of Lake Qinghai test, and obtains the calibration result. By comparing and analyzing the accuracy between primeval calibration result and site-calibration result using measurements data and Landsat5-TM, the result shows that the new calibration coefficients is better than 0.6%—3% in relative precision. Furthermore, the primeval calibration result has not satisfied remote sensing data's quantitatively application. The site-calibration method for B8 channel of HJ-1B is fit for calibration of sensor without observing cold space, and then, the calibration result accuracy satisfies the user thermal infrared data's quantitatively application.

REFERENCES

Berk A, Anderson G P, Acharya P K, Chetwynd J H, Bernstein L S, Shettle E P, Matthew M W and Adler-Golden S M. 1999. MODTRAN4 user's manual. MA: Air Force Research Laboratory

Biggar S F. 1990. In-flight methods for satellite sensor absolute radiometric calibration. Dissertation of Ph D, Tucson: the University of Arizona, U S A

Fang S H. Compiled 2009. Water Radiance Characteristic and Data Simulation. WuHan University Press

Flavio J P and Jurandir Z J. 2004. In-flight absolute calibration of the Landsat-5 TM on the test site salar de Uyuni .*Geoscience and remote sensing*. **42**(12): 2761—2766

Kurtis J T, Dennis L H and Aaron D. 2004. Landsat-5 TM and Landsat-7 ETM+ absolute radiometric calibration using the reflectance-based method. *Geoscience and remote sensing*. **42**(12): 2777—2785

Li H. Chief-editoring, 2001. Scientific Research Thesis Analects of China Remote Sensors Radiometric Calibration Site. Beijing: Ocean Press

Mayumi Y, Hiroshi MK and Yasushi M. 2005. Vicarious calibration of GLI by ground observation data. *Geoscience and remote sensing*. **43**(10): 2167—2176

Palmer J M. 1993. Calibration of satellite sensors in the thermal infrared. Proc. SPIE. 1762: l08—117

Richter R. 1997. On the in-flight absolute calibration of the spatial resolution space borne sensors using small ground targets. *International Journal of Remote Sensing*. **18**(3): 2827—2833

Simon J H, Gyanesh C, Julia A B and Ronald E. 2004. In-flight validation and recovery of water surface temperature with Landsat-5 thermal infrared data using an automated high-altitude lake validation site at Lake Tahoe. *Geoscience and remote sensing*. **42**(12): 2767—2776

Teillet P M, Slater P N and Ding Y. 1990. Three methods for the absolute calibration of the NOAA AVHRR sensor in-flight. *Remote Sensing of Environment*. **31**(2): 105—120

Tian G L. 2006. Thermal Remote Sensing. Beijing :Publishing House of Electronics Industry

Zhand Y. 2006. Study on thermal infrared remote sensors' absolutely radiometric calibrations. Dissertation of Ph D. Beijing: Institute of remote sensing applications,Chinese academy of science

Zhu L. 2008. Study of In-flight radiometric calibration and surface temperature retrieval for infrared camera. Dissertation of Ph D. Beijing: Institute of Remote Sensing Applications, Chinese Academy of Science

HJ-1B 热红外波段在轨绝对辐射定标

韩启金[1,2], 闵祥军[2], 傅俏燕[2]

1. 中国空间技术研究院, 北京 100081;
2. 中国资源卫星应用中心, 北京 100094

摘　要： 针对 HJ-1B 红外相机(IRS)热红外通道特点, 利用青海湖辐射校正场进行 HJ-1B 热红外绝对辐射定标, 提出新的场地定标算法, 并通过实测数据和 Landsat5-TM 数据对不同定标系数进行真实性检验分析, 发现该场地定标算法获得的系数比原始系数精度提高约 0.6%—3%, 总体精度为 1K 左右。研究结果表明文章提出的定标算法适用于不具备观测冷空间能力的卫星传感器在轨绝对辐射定标, 得到的定标系数合理可靠。

关键词： HJ-1B, 热红外, 场地定标, 精度

中图分类号： TP722.5　　　**文献标志码：** A

引用格式: 韩启金, 闵祥军, 傅俏燕. 2010. HJ-1B 热红外波段在轨绝对辐射定标. 遥感学报, **14**(6): 1212—1225
Han Q J, Min X J and Fu Q Y. 2010. In-flight absolute radiometric calibration for thermal infrared band of HJ-1B. *Journal of Remote Sensing*. **14**(6): 1212—1225

1 引　言

随着近年遥感技术的发展, 热红外遥感定量化应用也愈加广泛。对地热红外遥感昼夜工作的能力使其在环境污染、灾害监测、农业干旱监测和城市热岛研究等方面发挥着重要作用(田国良等, 2006)。我国于 2008-09-06 成功发射了环境与灾害监测预报小卫星星座(HJ-1A/B), 其中 HJ-1B 上搭载了一台红外多光谱相机(IRS), 其热红外波段(热红外)光谱范围 10.5—12.5μm, 空间分辨率 300m, 幅宽 720km, 重访周期 4 天, 可一定程度上满足我国热红外遥感定量化应用的需要。

遥感数据定量化应用的前提是传感器准确的绝对辐射定标, 即确定传感器输出信号(一般为卫星图像计数值 DN)与目标输入绝对物理量之间的定量关系(Palmer, 1993)。卫星传感器受发射时的振动、在轨空间环境变化和元器件老化等因素的影响, 其性能指标(如探测灵敏度)会发生改变, 定期的开展卫星传感器在轨辐射定标, 可以检验传感器性能变化情况, 修订原始定标结果从而满足遥感定量化应用的精度要求(Biggar, 1990)。

热红外在轨绝对辐射定标方法包括星上定标、交叉定标和场地定标。其中场地定标可以检验星上定标系统的稳定性, 修订星上定标结果的精度, 并在缺少交叉定标参考源的情况下完成传感器的在轨绝对辐射定标。目前热红外场地定标方法主要是利用海洋、湖泊、云等目标针对 Landsat5-TM、MODIS 传感器、FY 卫星等传感器提出的, 这些方法各有其特点和适用性(Richter, 1997; Teillet & Slater 等, 1990) 本文针对不具备观测冷空间能力的 HJ-1B IRS 特点, 利用 2009-08-12 青海湖场地试验数据对 HJ-1B 热红外通道进行场地定标, 获得适用于 HJ-1B IRS 特点的场地定标方法和 HJ-1B 热红外通道定标结果, 并通过青海湖实测数据和 Landsat5-TM 数据对定标结果进行验证分析, 结果表明青海湖场地定标结果精度可靠, 可满足用户开展遥感数据定量化应用需要。

2 场地定标算法

卫星传感器对定标场地(青海湖)进行观测时接收的辐射信号包括三部分: 第一部分是来自水表的辐亮度, 经过大气衰减到达卫星, 其大小由水体表层温度和比辐射率以及大气透射率共同决定; 第二部分是大气向上的辐亮度, 它与大气影响因子的含

收稿日期: 2009-12-07; 修订日期: 2010-04-08
基金项目: 国家重大科技专项工程(编号: 科工技[2006]785 号)。
第一作者简介: 韩启金(1983—) 男, 硕士, 主要从事卫星传感器定标和遥感定量化应用方面的研究工作。E-mail: cresda_hanjin@sina.com。

量和物理状态有关；第三部分是水表反射的大气向下辐亮度通过大气衰减到达卫星(张勇, 2006)。

HJ-1B 传感器接收的单色辐亮度可由下式计算得到:

$$L(\lambda)=L_{\text{lake}}(\lambda)\tau_a(\lambda)+L_{\text{up}}(\lambda)+\rho_{\text{lake}}(\lambda)\tau_a(\lambda)L_{\text{down}}(\lambda) \quad (1)$$

式中, $L(\lambda)$为卫星接收单色辐亮度, $\tau_a(\lambda)$为卫星观测路径整体大气透射率, $L_{\text{lake}}(\lambda)$为水体在卫星所在方向的辐亮度, $L_{\text{up}}(\lambda)$为卫星所在方向大气向上单色辐亮度, $\rho_{\text{lake}}(\lambda)$为水体的反射率, $L_{\text{down}}(\lambda)$为大气向下单色辐亮度。

由于青海湖水体可近似为黑体, 其中水体发射和反射的辐亮度可合并为一项 $L_{\text{lake2}}(\lambda)$, 用红外辐射计 CE312 测量获得, 则公式(1)可变为式(2)。

$$L(\lambda)=L_{\text{lake2}}(\lambda)\tau_a(\lambda)+L_{\text{up}}(\lambda) \quad (2)$$

卫星传感器接收的单色辐亮度还需要转化为通道辐亮度, HJ-1B 热红外通道入瞳处的等效辐亮度 L_e 可定义为:

$$L_e=\frac{\int L(\lambda)f_{\text{IRS}}(\lambda)\mathrm{d}\lambda}{\int f_{\text{IRS}}(\lambda)\mathrm{d}\lambda} \quad (3)$$

式中 $f_{\text{IRS}}(\lambda)$为 HJ-1B 热红外通道归一化的光谱响应函数。

HJ-1B 热红外通道输入信号和输出值间的关系按线性化研制设计, 可假设其通道辐亮度和卫星计数值之间的关系为式(4):

$$\text{DN}=g\cdot L_e+b \quad (4)$$

式中, DN 为卫星通道计数值, L_e 为通道辐亮度, 单位: $\text{W}\cdot\text{m}^{-2}\text{sr}^{-1}\mu\text{m}^{-1}$, 定标结果 g 为增益, b 为截距。卫星分别观测陆地和冷空间可得到两组数据, 根据公式(4)可求得定标结果 g 和 b, 由于 HJ-1BIRS 不具备观测冷空间的能力, 故采用星上高温校正黑体数据作为补充, 得到 HJ-1B 热红外场地定标整体流程(图1)。

3 HJ-1B 热红外场地定标

3.1 青海湖辐射校正场概况及数据测量

青海湖位于青藏高原东北部, 青海省境内, 是中国最大的内陆高原微咸水湖。整个湖区范围: 99°36′E—100°47′E, 36°32′N—37°15′N。青海湖面积 4473 km^2, 环湖周长 360 km, 湖面东西长 109 km, 南北宽 65 km, 平均水深 16 m, 最深处约 28 m, 湖面海拔 3196 m。青海湖地区属较高寒半干燥草原气候, 海拔较高, 大气干洁, 气溶胶粒子少, 水汽含量低, 卫星接收辐射信号大气订正量较小, 水面温度分布均匀, 是天然的热红外辐射校正场(李黄等, 2001)。

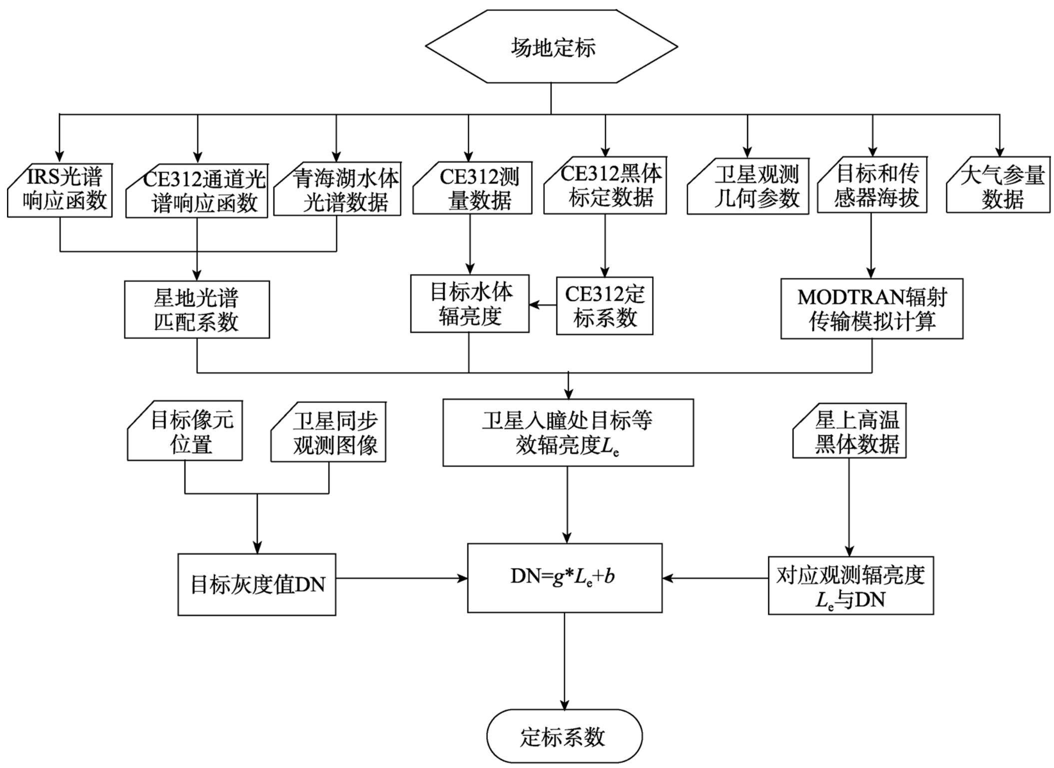

图 1 HJ-1B 热红外通道场地定标流程

HJ-1B 热红外波段场地定标试验测量数据包括青海湖水体辐亮度(CE312 测量)、水体热红外光谱数据(102F 测量)、水体温度数据(走航式水温仪)、GPS 数据、常规场地气象参数(探空仪测量)等。

3.2　CE312 水体辐亮度计算

3.2.1　辐射计黑体定标

辐射计 CE312黑体定标是通过一个可隐蔽的镀金反射镜，将目标的辐射量和光学内部的参考辐射量进行比较来完成。本次试验利用 Bman M340 型标准黑体对 CE312 进行定标，以 5F1t1M 的测量模式获得多组黑体定标数据。根据辐射计计数值与目标辐亮度关系式(5)拟合出 CE312 的定标系数 A、B。

$$L_s - L_m = A \times (DC_m - DC_s) + B \tag{5}$$

式中，DC_m 表示镜子插入光路时候辐射计的计数值，DC_s 表示镜子隐藏时候辐射计的计数值，L_s 表示目标(标准黑体)的辐亮度，L_m 表示反射镜的辐亮度。

黑体辐亮度 L_s 和反射镜辐亮度 L_m 通过标定黑体温度 T_s 和辐射计内部探头温度 T_m 利用 Plank 公式(6)和公式(7)求得。

$$L_\lambda = \frac{C_1}{\lambda^5 \left(e^{C_2/\lambda T} - 1 \right)} \tag{6}$$

$$L = \frac{\sum_{i=0}^{N} [L_\lambda \times (\lambda_{i+1} - \lambda_i) \times f(\lambda_i)]}{\sum_{i=0}^{N} [(\lambda_{i+1} - \lambda_i) \times f(\lambda_i)]} \tag{7}$$

式中，L_λ 为波长 λ 处对应黑体温度 T 下的辐亮度，$C_1=1.1904356\times10^{-6}$ W·m^{-2}, $C_2=1.4387685\times10^4$ μm·K，L 为仪器通道等效辐亮度，$f(\lambda_i)$ 为通道光谱响应函数。

针对 HJ-1B 热红外通道设置特点，仅需对 CE312 第 5 通道(B5:10.5—12.5μm)进行黑体标定。由于定标黑体为面源黑体，其比辐射率为 0.98±0.01，温度误差为±0.2°C，同时黑体液晶显示温度存在±0.2°C 左右的波动，单次标定数据确定的系数 A、B 会存在一定偏差，因此，进行黑体定标时，将多次定标测量的同温度下计数值放在一起，求得定标系数 A、B 的均值。青海湖试验所用红外辐射计 CE312-B5 通道黑体定标系数 A 为 0.0025，B 为 0.0184，单位: W·m^{-2}·sr^{-1}·μm^{-1}。

3.2.2　青海湖水体辐亮度计算

根据 CE312 黑体定标系数 A 和 B，对辐射计 CE312 同步测量青海湖辐亮度数据进行处理。利用辐射计计数值与目标辐射亮度之间的关系式(5)和公式(6)求得青海湖水体辐亮度 L_s 及对应的反演温度 T。由于测量过程中随机误差的存在，需将数据中的奇异点剔除。

(1) 将一个站位的 n 次目标测量数据进行计算，得出第五通道反演温度 T_i ($i=1,2,\cdots,n$)。

(2) 求出 n 次测量温度的平均值 T_a。

$$T_a = (\sum_{i=1}^{n} T_i) / n \tag{8}$$

(3) 求出反演温度 T_i 与平均温度值 T_a 的偏差的平均值 δT_a。

$$\delta T_a = (\sum_{i=1}^{n} |T_i - T_a|) / (n-1) \tag{9}$$

(4) 按照下式剔除偏差大的测量点。

$$\frac{|T_i - T_a|}{\delta T_a} \geqslant 3 \tag{10}$$

将剔除奇异点后的 CE312 数据反演温度与走航仪测量水体温度曲线进行对比，以检验 CE312 数据处理方法的正确性和精度。

青海湖 CE312 数据反演温度与走航仪测量温度曲线总体趋势一致，平均温度差异≤1.2°C(图 2)。

走航仪本身测温精度±0.02°C，试验时测温点位于水下约 0.5m，青海湖属微咸水质，水体温度在 8—10 月份出现逆温层现象，考虑到盐度、光照等因素影响，表层 0.5m 处温差小于 0.2°C(方圣辉，2009)。辐射计 CE312 测量时受水体反射影响，测量结果比实际水表辐射偏大，由于水体比辐射率约为 0.98，水体反射引起的反演温度误差较小。青海湖水质均匀面积较大，CE312 测量水域平均辐亮度精度≤0.6 W·m^{-2}·sr^{-1}·μm^{-1}，满足卫星传感器定标要求(朱利，2008)。对剔除奇异点之后卫星过境前后半小时的水表辐亮度进行均值化，得到同步测量水体辐亮度为 7.7289 W·m^{-2}·sr^{-1}·μm^{-1}。

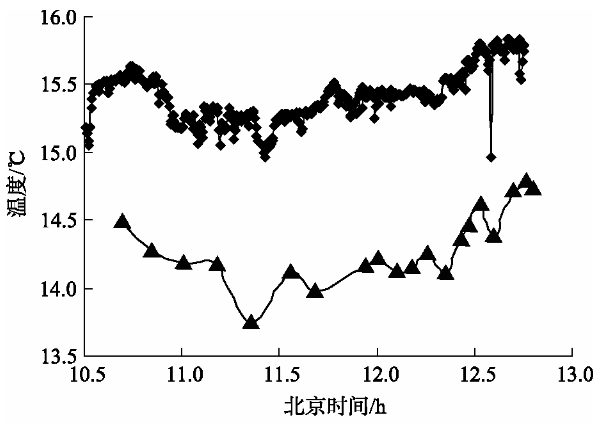

图 2　CE312 反演温度与走航仪测量温度对比图

3.3 星地光谱匹配

红外辐射计 CE312 的通道是模拟星载传感器光谱通道而设计，但与卫星本身通道光谱响应特性存在一定差异。因此，需对辐射计 CE312-B5 通道与 HJ-1B 热红外通道进行光谱匹配，以减少两者的光谱差异(图 3)。

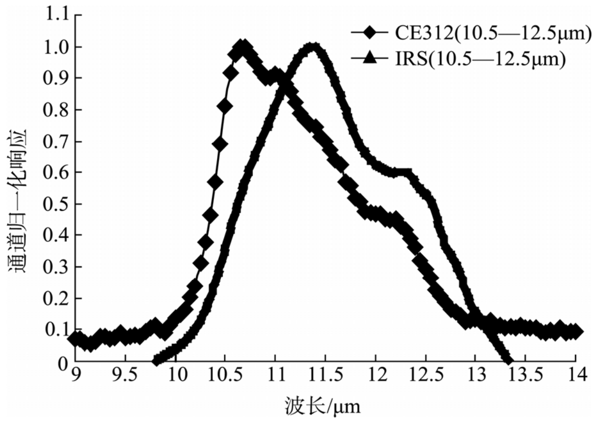

图 3 CE312 与 HJ-1B 热红外光谱响应对比

将 CE312-B5 通道光谱响应、HJ-1B 热红外通道光谱响应分别与青海湖热红外光谱辐亮度数据进行归一化，得到各自通道归一化辐亮度。再将两辐亮度的比值 k 作为星地光谱匹配因子修正 CE312 测量的水表辐亮度。具体计算公式如下所示:

$$R_{\mathrm{CE}}=\frac{\int L_{102\mathrm{f}}(\lambda)\times f_{\mathrm{CE}}(\lambda)\mathrm{d}\lambda}{\int f_{\mathrm{CE}}(\lambda)\mathrm{d}\lambda} \tag{11}$$

$$R_{\mathrm{IRS}}=\frac{\int L_{102\mathrm{f}}(\lambda)\times f_{\mathrm{IRS}}(\lambda)\mathrm{d}\lambda}{\int f_{\mathrm{IRS}}(\lambda)\mathrm{d}\lambda} \tag{12}$$

$$k=\frac{R_{\mathrm{IRS}}}{R_{\mathrm{CE}}} \tag{13}$$

式中，R_{CE} 和 R_{IRS} 分别是 CE312-B5 和 HJ-1B 热红外通道归一化辐亮度；$L_{102\mathrm{f}}(\lambda)$为青海湖水体热红外光谱辐亮度(102F 测量)；$L_{\mathrm{CE}}(\lambda)$和 $L_{\mathrm{IRS}}(\lambda)$分别为 CE312-B5 通道和 HJ-1B 星热红外通道光谱响应函数。

研究以傅里叶变换光谱仪 102F 测量的青海湖水体光谱辐亮度为基准，利用卫星过境前后 0.5h 内多次测量的光谱数据计算匹配因子，取其均值作为最终匹配因子。

HJ-1B 热红外通道的星地光谱匹配因子为 1.01；则考虑光谱匹配因子修订后的卫星入瞳处辐亮度计算公式为:

$$L_{\mathrm{e}}(\lambda)=k\times L_{\mathrm{lake2}}(\lambda)\times\tau_{a}(\lambda)+L_{\mathrm{up}}(\lambda) \tag{14}$$

3.4 MODTRAN 辐射传输计算

热红外通道场地定标试验，需要准确的测量卫星过境时刻的大气状况，获得同步测区的大气温湿压廓线及地表相关参数。考虑到试验条件的限制，在青海湖鸟岛宾馆附近于卫星过境时刻释放探空气球获取大气温湿压廓线。

分析试验探空数据得出卫星过境时刻大气温度、湿度和气压随海拔高度变化曲线(图 4)。

利用 MODTRAN4.0 辐射传输模型(Berk & Anderson 等，1999)，输入 HJ-1B 卫星同步观测路径几何参数、地面气象观测参数和大气温湿压廓线，模拟出分谱的大气透射率和大气向上辐亮度(图 5)。

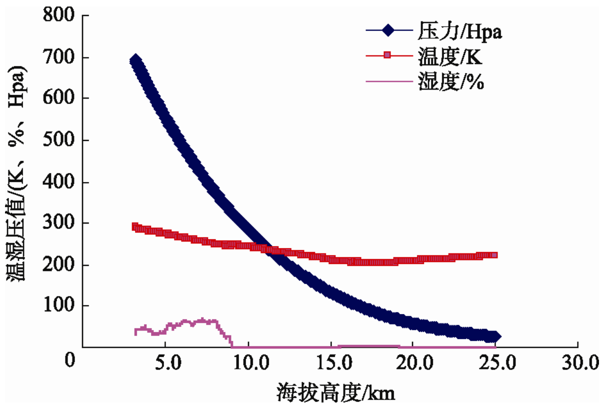

图 4 大气温湿压曲线

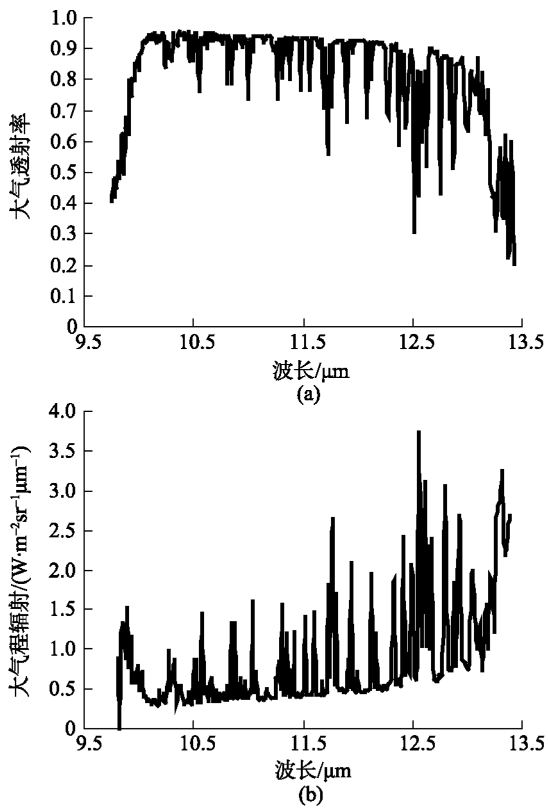

图 5 单色大气辐射传输曲线

(a) 单色大气透射率曲线; (b) 单色大气向上辐亮度曲线

将模拟结果分别与 HJ-1B 热红外通道光谱响应函数进行卷积，计算得到 HJ-1B 热红外通道的等效大气透射率为：0.8813(无单位)，大气向上辐亮度为 0.7225 $W \cdot m^{-2} \cdot sr^{-1} \cdot \mu m^{-1}$。

3.5　卫星计数值提取及定标结果计算

卫星通道计数值的提取，必须保证提取区域与测量区域的空间匹配精度。根据同步测量的空间范围确定计数值提取区域，对匹配区域的计数值进行均值化处理，以减少图像噪声的影响(Mayumi 等，2005)。

根据同步试验测量区域与图像的空间匹配情况，选定 HJ-1B 热红外图像上海心山(湖心白色斑点)东南部较深水域(根据 GPS 数据)提取相应 DN 值(图 6 中三角区为)。

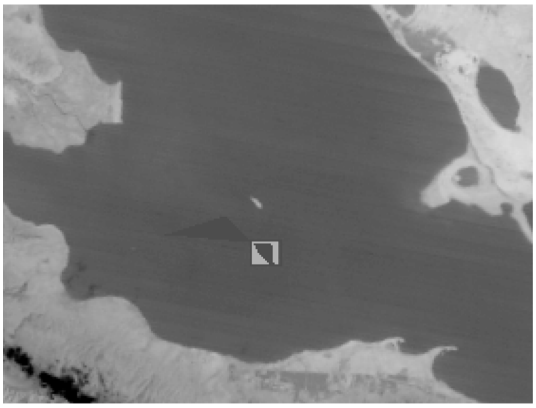

图 6　同步观测图像提取区域图

根据上述处理结果可得到 HJ-1B 热红外通道入瞳处等效辐亮度 L_e 和计数值 DN。HJ-1B IRS 观测冷空间时由于受太阳帆板的遮挡，无法获得冷空间数据，实验室对卫星观测冷空间过程采用等效 0 电平法去除反馈信号的影响，同时 HJ-1B IRS 探测性能采用了线性设计，因此采用单点法场地定标会引入较大不稳定误差。本文利用青海湖试验期间两天星上高温校正黑体数据作为补充，以提高定标结果线性拟合精度，完成 HJ-1B 热红外通道的场地定标。

根据 HJ-1B 星上定标系统原理，得到青海湖同步试验期间 HJ-1B 两天星上高温校正黑体数据处理结果(表 1)。

根据场地试验结果和星上数据计算出 HJ-1B 热红外通道在轨绝对辐射定标结果(公式(4))。其中增益 g 为 59.421 $W \cdot m^{-2} \cdot sr^{-1} \cdot \mu m^{-1}$；截距 b 为−25.441。

表 1　星上高温校正黑体数据计算结果

时间	2009-08-05		2009-08-14	
物理量	DN	辐亮度 /($W \cdot m^{-2} \cdot sr^{-1} \cdot \mu m^{-1}$)	DN	辐亮度 /($W \cdot m^{-2} \cdot sr^{-1} \cdot \mu m^{-1}$)
最小值	677.25	11.99	680.62	12.00
最大值	718.87	12.99	720.00	13.02
平均值	699.82	12.21	701.52	12.23

4　定标结果分析验证

4.1　定标结果精度检验

为了验证 HJ-1B 热红外通道场地定标结果精度，选择青海湖同步走航仪温度数据、浮标数据和 Landsat5-TM(10.5—12.5μm)数据对原始定标结果和新的场地定标结果进行交叉检验。

4.1.1　基于实测数据验证分析

利用原始定标结果和新的场地定标结果，分别定标 2009 年 8 月 12 日、16 日青海湖场地卫星遥感影像，得到不同定标结果下同步测区水表辐亮度 L_e，利用辐射传输模型法反演水表温度 T，并与同步实测温度数据进行比较。从而得到 HJ-1B 青海湖影像数据反演水体温度与实测温度间的差异(表 2)。

表 2　HJ-1B 反演温度与实测温度对比结果

/℃

数据获取时间	定标系数依据	反演通道温度	与走航仪温差	与浮标测量温差
8 月 12 日	原系数	15.99	0.65	1.14
	新系数	15.43	0.10	0.58
8 月 16 日	原系数	15.86	0.31	0.39
	新系数	15.28	0.27	0.19

4.1.2　基于 Landsat5-TM 数据分析

由于不同卫星同时相观测数据有限，本文采用青海湖 2009-08-11 HJ-1B 及 Landsat5-TM 数据进行对比分析，针对两卫星图像多个区域进行处理，图中同种颜色表示两卫星像间的匹配区域(图 7)，则可获得两颗卫星图像空间匹配区域对应 DN 值(表 3)。

表 3　HJ-1B 与 Landsat5-TM 图像匹配区域 DN 信息

选区号	HJ-1B 热红外图像提取 DN 信息			Landsat5-TM 图像提取 DN 信息		
	最小值	最大值	均值	最小值	最大值	均值
1	428	443	435.05	115	117	115.83
2	426	444	434.74	115	117	116.06
3	426	441	433.93	115	117	115.93
4	421	441	432.60	112	117	115.08
5	423	439	431.81	114	116	115.18

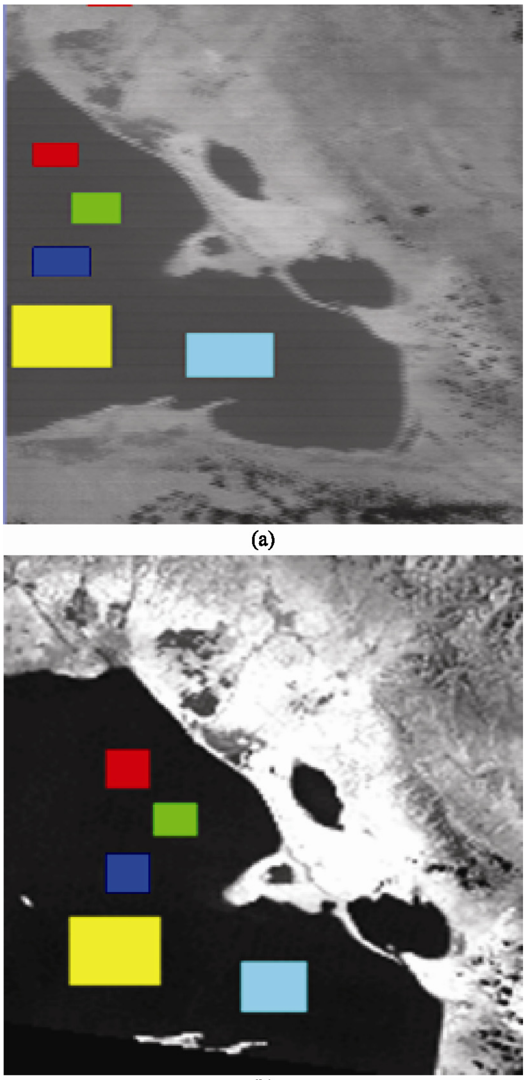

(a)

(b)

图 7 HJ-1B 图像与 landsat5-TM 图像空间匹配
(a) HJ-1B 图像; (b) Landsat5-TM 图像

根据 Landsat5-TM 卫星头文件中相关数据可以求得绝对辐射定标公式(15)。

$$L_e = \frac{(L_{max} - L_{min})}{255} \times DN + L_{min} \tag{15}$$

式中, L_{max}=15.303, L_{min}=1.238, L_e为卫星通道辐亮度。

根据匹配区域 DN 信息可求得卫星图像对应的辐亮度和反演温度(公式 4、6、15)为提高验证精度, 对匹配区域的辐亮度与反演温度进行均值化处理, 并将不同定标结果下 HJ-1B 热红外数据辐亮度和反演温度与 Landsat5 TM 数据进行对比(表 4)。

表 4 不同数据源对应辐亮度与反演温度比较

数据获取途径	原始系数标定	场地系数标定	Landsat5-TM
辐亮度/($W \cdot m^{-2} \cdot sr^{-1} \cdot \mu m^{-1}$)	7.7795	7.7257	7.6150
反演温度/°C	15.18	14.73	14.15
辐亮度方差	0.00052	0.00055	0.00062

HJ-1B 过境青海湖时刻与 Landsat5 相差 12 分钟, 由于青海湖为微咸均匀水质, 面积较大, 可认为水表温度短时间内恒定。两卫星波段相近, 可通过比较通道接收辐亮度差异和反演温度差异来验证 HJ-1B 定标精度(Flavio & Jurandir, 2004), 结果表明场地定标系数对应定量产品与 Landsat5-TM 产品差异较小, 考虑到 Landsat5-TM 本身定标精度为 0.5K(Kurtis & Dennis 等, 2004), 确定 HJ-1B 星热红外总体定标精度约为 1K(表 4)。

4.2 不同定标结果精度分析

4.2.1 原始定标精度分析

HJ-1B 热红外原始定标结果是利用 2008 年星上黑体定标获得, 星上定标沿用发射前实验室获得的计算公式, 本身存在一定的误差。卫星传感器受到在轨空间环境和元器件老化等影响, 定标系统和探测性能发生衰变, 原始的定标结果已无法准确的反映 HJ-1B IRS 输出信号与输入信号的定量关系, 其定标精度需要进行修订。

4.2.2 场地定标精度分析

HJ-1B 热红外通道场地定标精度受多种因素的影响, 首先青海湖水表光谱辐射随时间和温度产生波动(图 8), 一定波长处辐亮度 1 小时内波动差异 0.5 $W \cdot m^{-2} \cdot sr^{-1} \cdot \mu m^{-1}$ 左右。辐射计 CE312-B5 通道和 HJ-1B 星热红外通道光谱响应函数的变化以及光谱匹配基准波动的存在, 使得光谱匹配因子产生相应的误差(Simon 等, 2004)。

其次传感器探测性能稳定性问题使得星上校正黑体温度存在±2°C 波动, 引起辐亮度 0.02 $W \cdot m^{-2} \cdot sr^{-1} \cdot \mu m^{-1}$ 左右的变化和通道计数值 2DN 左右的波动, 因此星上高温校正黑体数据也给 HJ-1B 星热红外通道场地定标结果带来一定误差。

4.2.3 定标结果精度对比

根据验证结果(表 2 和表 4), 分析 HJ-1B 热红

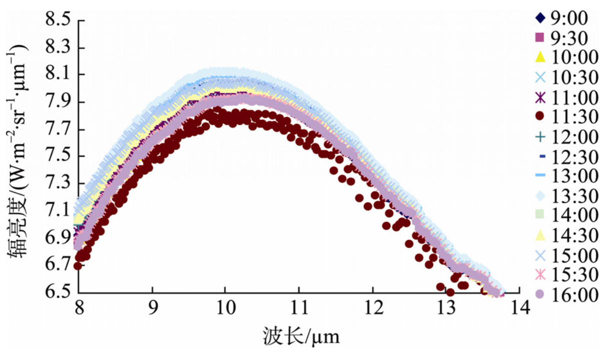

图 8 青海湖测量水体辐射量波动曲线

外通道场地定标结果与原始定标结果的相对精度变化。

HJ-1B 热红外通道的场地定标结果比原始定标结果相对精度提高约 0.6%—3%左右(表 5), 进一步证明 HJ-1B IRS 在轨运行过程中探测性能发生了变化, 必须对发布的定标结果进行定期修订。

表 5 试验前后绝对辐射定标结果精度对比

/%

精度对比验证方法	原始定标结果精度	场地定标结果精度	精度提高
实测数据验证	3.21	2.57	0.64
Landsat5-TM 验证	7.32	4.10	3.22

5 结 论

利用青海湖辐射校正场对 HJ-1B 热红外通道进行了绝对辐射定标, 获得对应的绝对辐射定标结果。通过实测数据和 Landsat5 TM 数据对 HJ-1B 热红外通道场地定标和原始定标的精度进行对比验证, 结果表明 HJ-1B 热红外通道场地定标结果精度 1K 左右, 比原始结果相当精度提高约 0.6%—3%, 进一步说明 HJ-1B IRS 受环境和元器件老化的影响, 探测性能发生了衰变, 原始定标结果已无法满足数据定量化应用精度要求。本文提出的 HJ-1B 热红外通道场地定标方法, 适用于不具备观测冷空间能力的传感器场地定标, 得出的 HJ-1B 热红外通道场地定标结果精度满足用户开展 HJ-1B 热红外数据定量化应用需要。

REFERENCES

Berk A, Anderson G P, Acharya P K, Chetwynd J H, Bernstein L S, Shettle E P, Matthew M W, and Adler-Golden S M. 1999. MODTRAN4 user's manual. MA: Air Force Research Laboratory

Biggar S F. 1990. In-flight methods for satellite sensor absolute radiometric calibration. Dissertation of Ph D, Tucson: the University of Arizona, U S A

Fang S H. 2009. Water Radiance Characteristic and Data Simulation, compiled WuHan University Press

Flavio J P and Jurandir Z J. 2004. In-flight absolute calibration of the Landsat-5 TM on the test site salar de Uyuni .*Geoscience and remote sensing*. **42**(12): 2761—2766

Kurtis J T, Dennis L H and Aaron D. 2004. Landsat-5 TM and Landsat-7 ETM+ absolute radiometric calibration using the reflectance-based method. *Geoscience and remote sensing*. **42**(12): 2777—2785

Li H. 2001. Scientific Research Thesis Analects of China Remote Sensors Radiometric Calibration Site. Beijing: Ocean Press

Mayumi Y, Hiroshi MK and Yasushi M. 2005. Vicarious calibration of GLI by ground observation data. *Geoscience and remote sensing*. **43**(10): 2167—2176

Palmer J M. 1993. Calibration of satellite sensors in the thermal infrared. Proc. SPIE. 1762: l08—117

Richter R. 1997.On the in-flight absolute calibration of the spatial resolution space borne sensors using small ground targets. *International Journal of Remote Sensing*. **18**(3): 2827—2833

Simon J H, Gyanesh C, Julia A B and Ronald E. 2004. In-flight validation and recovery of water surface temperature with Landsat-5 thermal infrared data using an automated high-altitude lake validation site at Lake Tahoe. *Geoscience and remote sensing*. **42**(12): 2767—2776

Teillet P M, Slater P N and Ding Y. 1990. Three methods for the absolute calibration of the NOAA AVHRR sensor in-flight. *Remote Sensing of Environment*. **31**(2): 105—120

Tian G L. 2006. Thermal Remote Sensing. Beijing :Publishing House of Electronics Industry

Zhang Y. 2006. Study on thermal infrared remote sensors' absolutely radiometric calibrations. Dissertation of Ph D. Beijing: Institute of remote sensing applications,Chinese academy of science

Zhu L. 2008. Study of In-flight radiometric calibration and surface temperature retrieval for infrared camera. Dissertation of Ph D. Beijing: Institute of Remote Sensing Applications, Chinese Academy of Science

附中文参考文献

方圣辉. 2009.自然水体辐射特性与数值模拟. 武汉大学出版社

李黄. 2001. 中国遥感卫星辐射校正场科研成果论文选编.北京: 海洋出版社

田国良. 2006. 热红外遥感. 北京: 电子工业出版社

张勇. 2006. 遥感传感器热红外数据辐射定标研究. 中国科学院遥感应用研究所博士研究生学位论文

朱利. 2008. 热红外辐射定标及地表温度反演研究. 中国科学院遥感应用研究所博士研究生学位论文